The Seismic Record
A journal of the Seismological Society of America

Potency–Magnitude Scaling Relations and a Unified Earthquake Catalog for the Western United States

Daniel T. Trugman*[1] and Yehuda Ben-Zion[2]

Abstract

Quantifying the size of earthquakes is a foundational task in seismology, and over the years several magnitude scales have been developed. Of these, only scales based on seismic moment or potency can properly characterize changes in event size without saturation. Here, we develop empirical potency–magnitude scaling relations for earthquakes in the western United States, allowing us to translate instrumental magnitude estimates into uniform measures of earthquake size. We use synthetic waveforms to validate the observed scaling relations and to provide additional insight into the differences between instrumental and physics-based magnitude scales. Each earthquake in our catalog is assigned a clustering designation distinguishing mainshocks from triggered seismicity, along with a potency-based magnitude estimate that is comparable to moment magnitude and that can be easily converted into other magnitude scales as needed. The developed catalog and associated scaling relations have broad applications for fundamental and applied studies of earthquake processes and hazards.

Cite this article as Trugman, D. T. and Y. Ben-Zion (2024). Potency–Magnitude Scaling Relations and a Unified Earthquake Catalog for the Western United States, *The Seismic Record*. **4**(**3**), 223–230, doi: 10.1785/0320240022.

Supplemental Material

Introduction

Magnitude is the most widely used and societally relevant earthquake source parameter. Larger earthquakes have overall greater damage potential, and thus an accurate characterization of earthquake size is of great interest to both seismologists and the public. Despite this fundamental importance, accurately measuring earthquake size is challenging because of the attenuation of seismic waves as they propagate from the earthquake rupture process at depth to geophysical sensors at the surface. Additional complications arise from the strong structural heterogeneities around faults and at shallow depths. These issues render it impossible to resolve fine details of earthquake ruptures, but robust information on the size of earthquakes can be obtained from analysis of low-frequency seismic waves. In this article, we develop a unified earthquake catalog for the western United States, including uniform magnitude estimates derived from seismic potency—a fundamental source parameter (the product of fault area and average slip) that controls the amplitude of low-frequency seismic waves.

Over the years, numerous techniques have been developed to measure earthquake size. In pioneering work, Charles Richter (1935) defined a measure of earthquake size by correcting for the systematic decay with distance of waveform amplitudes recorded on Wood–Anderson seismometers in southern California. The measurement, now called local magnitude (M_L), is still widely used by regional monitoring networks due to its simplicity and applicability to small and frequently recorded earthquakes. Building on this work, Beno Gutenberg demonstrated how body- (Gutenberg, 1945a) and surface-wave (Gutenberg, 1945b) amplitudes could be analyzed similarly but at greater distances to create body- and surface-wave magnitude scales (M_b and M_s) of particular relevance for larger earthquakes. For small earthquakes, it can sometimes be advantageous to use duration rather than

1. Nevada Seismological Laboratory, Nevada Geosciences, University of Nevada, Reno, Reno Nevada, U.S.A., https://orcid.org/0000-0002-9296-4223 (DTT); 2. Department of Earth Science and Statewide California Earthquake Center, University of Southern California, Los Angeles, California, U.S.A., https://orcid.org/0000-0002-9602-2014 (YB-Z)

*Corresponding author: dtrugman@unr.edu

amplitude as a basis for calculating magnitude, with coda duration magnitudes (M_D) being the most popular such metric (Aki, 1969; Herrmann, 1975; Bakun and Lindh, 1977). For any magnitude scale, it is important to recognize that different monitoring agencies can have different data processing procedures or apply different empirical correction functions, which can lead to slight differences in the magnitude estimates depending on the authors; see Bormann and Dewey (2014) for a detailed review.

Despite their utility, all these metrics are instrumental magnitudes derived from properties of seismic records that only indirectly correspond to properties of the earthquake source. This correspondence is imperfect because all instrumental magnitudes are known to saturate, failing to increase in parity with increases in earthquake size (Kanamori, 1977). For this reason, the community has moved to a preference for magnitudes derived from seismic moment M_0, which is a parameter with units of energy defined as the product of a nominal rigidity, fault area, and average slip (e.g., Aki, 1972). Kanamori (1977) used empirical energy scaling relations to define a moment magnitude parameter M_w that can be written as

$$M_w = \frac{2}{3}(\log_{10} M_0 - 16.1), \quad (1)$$

with M_0 measured in dyn · cm. Building on this work, Hanks and Kanamori (1979) defined a related moment magnitude parameter **M** based on the coincidence of magnitude scales for moderate-to-large earthquakes as

$$\mathbf{M} = \frac{2}{3}\log_{10} M_0 - 10.7. \quad (2)$$

There is a slight difference in these two definitions of moment magnitude, as $M_w \sim \mathbf{M} - 0.0333$. In this work, we use equation (1) and the notation M_w to define moment magnitude.

Direct estimation of M_w is often challenging for smaller earthquakes due to the requirement for sufficient signal-to-noise ratios at the long periods used in waveform inversions. As a result, many earthquake catalogs contain a mixture of different magnitude types, with local and duration magnitudes (M_L and M_D) dominant for small events and moment magnitudes (M_w) prevalent for large ones. This heterogeneity can be problematic, particularly for interpreting earthquake statistics, frequency–magnitude distributions, and scaling of ground motion with magnitude, all of which are central to seismic hazard analysis (e.g., Herrmann and Marzocchi, 2020).

The objective of this study is to develop a uniform, physics-based, and self-consistent catalog of event sizes for historic and modern earthquakes in the western United States. To do this, we leverage the data from the U.S. Geological Survey's (USGS) Comprehensive Catalog (ComCat), for which many individual events have multiple magnitude estimates of distinct types, allowing us to develop empirical relations between different magnitude types. We validate these magnitude scaling relations with synthetic waveforms generated via the stochastic method (Boore, 2003), for which the earthquake size is known by definition and various measures can be readily extracted for comparison. Our work extends classic research on magnitude scaling relations (e.g., Thatcher and Hanks, 1973; Bakun, 1984; Hanks and Boore, 1984) but with a greatly expanded sample of data.

In this work, we use seismic potency P_0, which has units of volume (e.g., Ben-Zion, 2003), as our target size parameter. The more commonly used seismic moment M_0 is given by P_0 multiplied by an assumed rigidity at the source. However, the definition of seismic moment can be ambiguous because rigidity can change discontinuously across faults, and elasticity breaks down in rupture zones, making the rigidity at the source ill-defined for earthquakes. Moreover, observed ground motions can be fully parameterized in terms of motions at the boundaries of the source volume that propagate from there in the form of elastic waves. The failure processes and rigidity in the source volume are completely accounted for by their action at the boundaries, so the nominal rigidity used to define M_0 is an extra parameter that can create ambiguity in source characterization (Ben-Zion, 1989, 2001).

This study provides self-consistent and physics-based estimates of both potency- and moment-based earthquake magnitudes in the western United States that can be used for various research topics. For example, Mueller (2018) described a methodology for compiling a uniform earthquake catalog for the 2023 United States National Seismic Hazard Map using magnitude conversion relations derived from Utsu (2002) based on a legacy compilation of global data. The conversion relations developed in this study could be easily incorporated for this purpose and are based on a much larger and updated compilation of data specific to the western United States. As shown subsequently, the data require conversion relations that are quadratic rather than linear as is often assumed.

Data and Methods

We analyze earthquake magnitude estimates listed in the USGS's ComCat. Our study region encompasses the

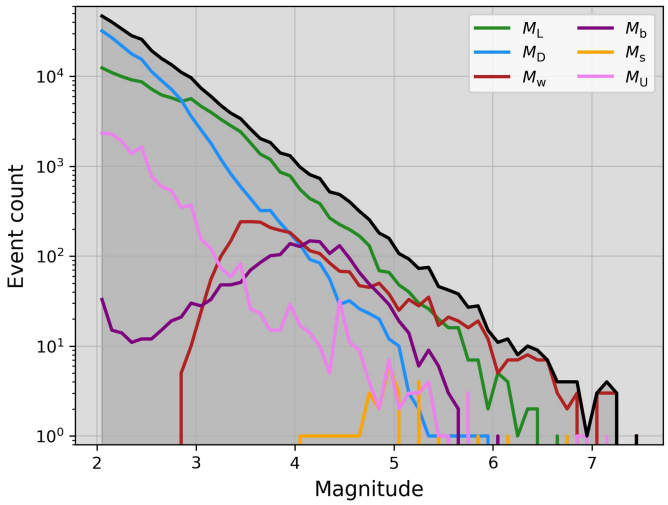

Figure 1. Frequency–magnitude distributions for different ComCat-preferred magnitude types of western U.S. earthquakes (1950–2024). For small earthquakes, local and duration magnitudes (M_L and M_D) predominate, whereas for larger events, moment magnitudes M_w, body-wave magnitudes M_b, or occasionally surface-wave magnitudes M_s are usually preferred if available. A small fraction of events, mostly small ones, have unknown, helicorder or another nonstandard magnitude type (M_U). The composite distribution combining all of the preferred magnitude types is shown in black for reference.

continental western United States (longitudes: from −128.0° to −109.0°, latitudes: 31.0° to 49.5°) from January 1950 to June 2024. For each unique event, ComCat lists a preferred origin and magnitude estimate, and we focus on events with preferred magnitudes 2.0 and greater (314,925 events in total). The preferred magnitudes are highly variable in type (Fig. 1); most small events list M_L or M_D as the preferred magnitude, whereas M_b, M_s, and M_w are increasingly prevalent for larger events (ComCat uses equation 1 and not equation 2 to define moment magnitude). The frequency–magnitude statistics depend on the type of magnitude used in the data compilation, as noted in previous studies (e.g., Shelly *et al.*, 2021). This variability compromises any characterization of magnitude statistics; it is remarkable that mixing all these distributions, as is done in many studies, leads to an approximate power-law distribution over most of the magnitude range.

Our purpose here is to unify these data via a magnitude scale based on seismic potency. To do this, we use the multiple magnitude estimates for individual events in ComCat, obtained from different sources or different methods, to develop statistical relations that connect different magnitude types. For example, to obtain a conversion relation between moment and local magnitude, one could focus on the subset of events with at least one magnitude estimate of both types. Our approach focuses on developing scaling relations for seismic potency P_0 in log units (Ben-Zion and Zhu, 2002; Ross *et al.*, 2016) and then reporting uniformly $\log_{10} P_0$ and related magnitudes. The scaling relations between $\log_{10} P_0$ and other magnitude scales can be used to derive those magnitudes in situations where this is desirable. In general, there will be a different potency scaling relationship for each magnitude type. We present the method in detail for M_L versus $\log_{10} P_0$ subsequently; scaling relations for other magnitude types are shown in the supplemental material available in this article.

To develop the potency–magnitude scaling relation, we begin by compiling M_w and M_L estimates for all events in the dataset that contain at least one estimate of both magnitude types. Because M_w can only be reliably estimated for moderate-to-large events, this dataset only includes events of this size range. Some events contain more than one estimate of M_w or M_L, and in these cases, we take the preferred ComCat value if available (i.e., if M_w or M_L is the preferred magnitude type) and the median value otherwise. With the selected magnitude estimates in hand, we transform M_w into moment (in units of dyn · cm) and then compute potency using the following relations (e.g., Ben-Zion, 2003):

$$\log_{10} M_0 = 1.5 M_w + 16.1, \tag{3}$$

$$\log_{10} P_0 = \log_{10} M_0 - \log_{10} \mu - 11. \tag{4}$$

We assume a nominal rigidity μ of 36 GPa consistent with average crustal values used in regional moment tensor inversions for earthquakes in the western United States (e.g., Ichinose *et al.*, 2003). The units of potency here are centimeters per square kilometer, a convenient choice because most earthquakes in the dataset have average slips and fault areas of the order of centimeters and square kilometers, respectively. The value of 11 on the right side of equation (4) accounts for the unit conversion from M_0 in dyn · cm.

Next, we use linear regression techniques to develop statistical relations between $\log_{10} P_0$ and M_L. To prevent small earthquakes (which are more frequent) from dominating the model fit, we first bin the data by magnitude and compute the median potency and magnitude value in each bin. Analyzing the median trends rather than individual data points also improves the robustness of the results, given that the magnitude estimates (especially for nonpreferred magnitudes) can be

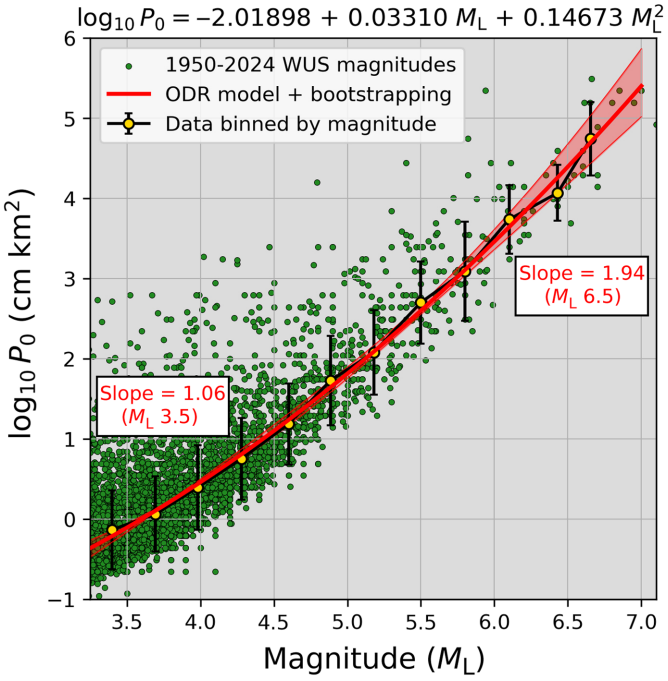

Figure 2. Scaling of potency with local magnitude for earthquakes in the western United States. Earthquakes from ComCat (green circles) are binned by M_L, and orthogonal distance regression (ODR) is performed on the median *x* and *y* values in each bin (gold circles). The fitted ODR model and prediction uncertainty obtained from bootstrapping are displayed as a red line and shading.

highly uncertain. We fit the binned data to a quadratic model of the form:

$$\log_{10} P_0 = c_0 + c_1 M_L + c_2 M_L^2, \quad (5)$$

using orthogonal distance regression (Boggs and Rogers, 1990) to account for uncertainties in both M_L and $\log_{10} P_0$ values. Uncertainties in the fit are obtained from bootstrap resampling the data and rebinning 10,000 times (Efron and Tibshirani, 1994).

Results

Though there is considerable scatter from event to event, we observe a systematic increase in median seismic potency values (parameterized as $\log_{10} P_0$) with local magnitude M_L (Fig. 2). This trend is nonlinear but is well described by the quadratic model of equation (5), with the local slope of the fitted model ($c_1 + 2c_2 M_L$) increasing from ~1.0 at M_L 3.5 to ~2.0 at M_L 6.5. This steepening of the curve can be interpreted in terms of magnitude saturation: any instrumental measure of earthquake magnitude derived from a finite-frequency band will fail at some event size to capture true increases in earthquake magnitude (Kanamori, 1977). The change in the local slope may also reflect at least partially a transition in the physics governing small and large events (Ben-Zion and Zhu, 2002). It is difficult to comprehensively compare our model to previous studies on magnitude scaling relations because the underlying data and functional forms of the models differ. However, a slope of order 1.5 seems to be the general consensus for moderate earthquakes (Thatcher and Hanks, 1973; Bakun, 1984; Ben-Zion and Zhu, 2002) and is also consistent with the definition of M_w. Because our data are concentrated between M_L 3.5 and 6.0, the uncertainties in the model predictions become large outside this range (Fig. S1). In particular, although the potency–magnitude scaling fit well by quadratic function within this range of event sizes, extrapolation of the model beyond these bounds may not be viable. We discuss this issue in greater detail subsequently.

The USGS ComCat catalog features several different preferred magnitude types; therefore, it is desirable to generalize this analysis to include other magnitude scales. We repeat this same basic procedure for M_D, M_b, and M_s (Fig. S2), with corresponding model coefficients and uncertainties listed in Table 1 alongside those for M_L. Similar to the results for M_L, we observe that the scaling of M_D with potency is best described by a quadratic model that steepens (saturates) with increasing magnitude. In contrast, for M_b and M_s, the potency–magnitude scaling is well described by a linear model, though the M_s relation is more precise (Fig. S2). The approximately constant slope (lack of saturation) for M_b and M_s is likely an observational bias because there are very few of the large (M_w 7–8) events in our dataset where changes in slope could become clear.

Discussion

The scaling of instrumental magnitudes with seismic potency (or more commonly, moment) is a classic problem in seismology that we revisit in this study, armed with a large data set that spans a broad range of event sizes. Hanks and Boore (1984) developed a conceptual model of the scaling of local magnitude and seismic moment in terms of the natural frequency of the Wood–Anderson seismograph (f_s), the corner frequency of the earthquake (f_0), and near-surface attenuation (f_{max}). They identified three regimes: (1) for large earthquakes with f_0 much less than f_s, the scaling should be $\log_{10} M_0 \sim 3.0 M_L$, (2) for moderate earthquakes for which f_0 is much greater than f_s but less than f_{max}, the scaling should be $\log_{10} M_0 \sim 1.5 M_L$, and for small earthquakes with f_0 greater than f_{max}, the scaling should be $\log_{10} M_0 \sim 1.0 M_L$. Our results are qualitatively

Table 1
Potency and Magnitude Scaling Coefficients

Scaling Relation	c_0	c_1	c_2	Magnitude Range
$\log_{10} P_0(M_L)$	−2.01898	0.03310	0.14673	M_L 3.5–7.0
	−3.81636	1.06018	*n/a*	M_L 2.0–3.5
$\log_{10} P_0(M_D)$	−1.93775	0.00672	0.15463	M_D 3.5–7.0
	−3.83193	1.08912	*n/a*	M_D 2.0–3.5
$\log_{10} P_0(M_b)$	−6.70743	1.79490	*n/a*	M_b 4.0–6.5
$\log_{10} P_0(M_s)$	−3.22427	1.16261	*n/a*	M_s 3.5–7.0
M_P (M_L)	2.29155	0.02207	0.09782	M_L 3.5–7.0
	1.09329	0.70679	*n/a*	M_L 2.0–3.5
M_P (M_D)	2.34570	0.00448	0.10308	M_D 3.5–7.0
	1.08291	0.72608	*n/a*	M_D 2.0–3.5
M_P (M_b)	−0.83409	1.19660	*n/a*	M_b 4.0–6.5
M_P (M_s)	1.48802	0.77507	*n/a*	M_L 3.5–7.0

For each magnitude type M_i, we fit a general model of the form listed in equation (5) in the Data and Methods section: $\log_{10} P_0 = c_0 + c_1 M_i + c_2 M_i^2$. For M_b and M_s, the quadratic coefficient c_2 is not estimated as the scaling appears linear within the applicable magnitude range given in the rightmost column. Similarly, we assume a linear scaling for M_L and M_D for small events below the domain of the binned data of Figure 2 and Figure S2. The bottom portion of table uses equation (6) to translate from $\log_{10} P_0$ to M_P, resulting in an analogous equation: $M_P = c_0 + c_1 M_i + c_2 M_i^2$. To good approximation, M_P and M_w can be used interchangeably, and equation (7) can be applied to obtain M_w from M_P when the assumed rigidity value to calculate moment is substantially different than the default value of 36 GPa.

compatible with this model; the slope of the scaling for small earthquakes is about 1 and increases systematically with event size. However, the steepest possible scaling compatible with the data is ∼2.0–2.4 for large events (Fig. 2, Fig. S1), never approaching the hypothesized value of 3.0. Hanks and Boore (1984) noted a similar trend in their dataset but attributed it to lack of observations; revisiting this problem 40 yr later with a much-expanded catalog makes this explanation less compelling.

To study this problem further, we generated synthetic waveforms from earthquakes of known potency using the stochastic method (Boore, 1983), for which each synthetic waveform is a random realization of the target spectrum that combines modeled source, path, and site effects on ground motion. Here, we use a seismological model emulating the work of Yenier and Atkinson (2015) that includes a non-self-similar, generalized double-corner model of the source spectrum, a transition from body- to surface-wave geometric spreading with distance, frequency-dependent attenuation, and both site amplification and attenuation effects (see Text S1 for additional details). Hanks and Boore (1984) applied a similar approach but with a simplified parameterization of source, site, and path effects. A major advantage of the Yenier and Atkinson (2015) model parameterization is that it was calibrated to match ground motion observations of the California earthquakes that comprise most of our dataset, lending confidence to its application in this context (see also Fig. S3). The stochastic simulations are designed for class B/C site conditions; we neglect here the amplification of individual sites relative to this reference condition because we are mainly interested in magnitude scaling.

We generate synthetic waveforms for M_w 2–7 earthquakes at a range of distances up to 300 km, convert the acceleration time series into Wood–Anderson displacement and derive M_L from the peak amplitude corrected for distance (Hutton and Boore, 1987). The results, aggregated across hundreds of thousands of simulations, are presented in Figure 3. The scaling of $\log_{10} P_0$ with M_L is quadratic with comparable scaling coefficients, if slightly steeper, than the model coefficients obtained from observational data (Fig. 2). Although the stochastic method assumes a simplified representation of the earthquake process, it provides a useful conceptual basis for understanding the magnitude scaling of ground motion observed in nature. In particular, it is noteworthy that saturation effects for M_L can be replicated using existing seismological models of source, path, and site effects without modification.

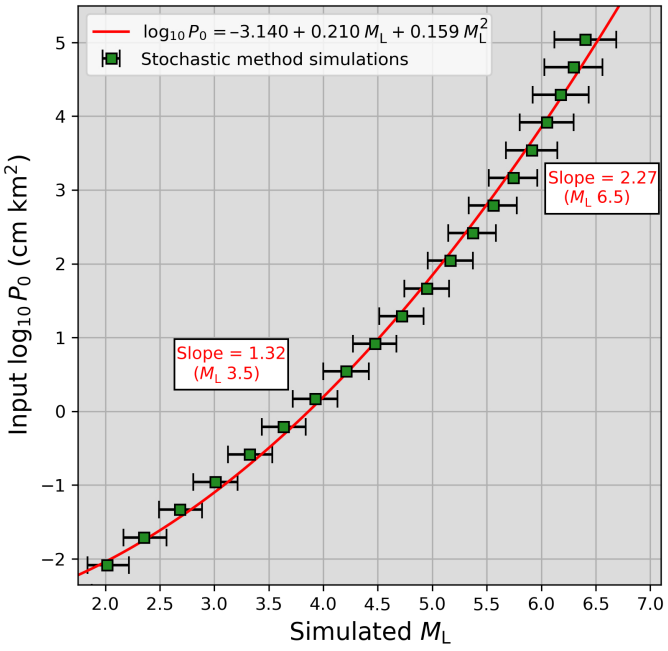

Figure 3. Potency–magnitude scaling relations derived from synthetic waveforms obtained via the stochastic method. Synthetic waveforms from earthquakes of known potency are simulated at a range of distances up to 300 km and M_L is estimated from the peak Wood–Anderson displacement amplitude, corrected for distance. A quadratic scaling relation is fitted using orthogonal distance regression to the median M_L values, analogous to the treatment of the observational data in Figure 2. The scaling curve derived from the synthetics is slightly steeper than in the natural dataset but is otherwise comparable in functional form.

An important outcome of this study is the capability to develop a uniform set of magnitude estimates derived from seismic potency for earthquakes in the western United States. To do this for our ComCat dataset, we estimate potency either directly from moment when possible or using the scaling relations listed in Table 1 applied to the ComCat preferred magnitudes. About 5% of events list a preferred magnitude type other than M_L, M_D, M_b, M_s, or M_w. Nearly all of these are small events with "helicorder" magnitudes that we assume for these calculations approximate M_L. Rather than extrapolate our quadratic models for M_L and M_D beyond the support of the fitted data (i.e., below magnitude ~3.5), we assume a transition from quadratic to linear scaling of $\log_{10} P_0$ with magnitude for small earthquakes (see Table 1 for details). This assumption is consistent with the conceptual model of Hanks and Boore (1984) and also with the work of Ross *et al.* (2016), who observed a linear scaling for small earthquakes in the San Jacinto fault zone. Similarly, for $M_b < 4$, we first convert to M_L (Fig. S4) and apply the appropriate relation to estimate potency. Though beyond the scope of this study, future efforts could be dedicated to refining potency–magnitude scaling relations for small earthquakes.

With potency values estimated for all earthquakes following this procedure, we can define a potency magnitude M_P by combining equations (3) and (4):

$$M_P \equiv \frac{2}{3}(\log_{10} P_0 + 5.4563), \tag{6}$$

in which potency is measured in centimeters per square kilometer. By design, M_P is equivalent to M_w (equation 1), assuming that a rigidity μ_0 of 36 GPa is used in the calculation of M_0. For other choices of μ, M_P can be easily converted into M_w by shifting according to the assumed rigidity μ:

$$M_w = M_P + \frac{2}{3}\log_{10}\left(\frac{\mu}{\mu_0}\right). \tag{7}$$

For many applications, this adjustment is likely to be small, and thus M_P and M_w could be used interchangeably. Unlike instrumental magnitude scales, the M_P and M_w magnitudes do not saturate and can be used in applications for which a uniform and physically consistent magnitude scale is desired. Alternatively, if one desires estimates of instrumental magnitudes like M_L, it is possible to invert the developed scaling relations to translate potency into the magnitude type of interest. For convenience, we provide conversion relations from $\log_{10} P_0$ and M_P to different magnitude scales in Table 1. The catalog also includes clustering designations for each earthquake based on the nearest-neighbor method (Zaliapin and Ben-Zion, 2013), which can be useful for some applications.

It is illuminating to compare the frequency–magnitude distribution for M_P with the equivalent distribution of preferred magnitudes listed by ComCat (Fig. 4). The two distributions are similar for larger events but differ markedly for smaller earthquakes where the ComCat preferred magnitude systematically underestimates M_P. The apparent simplicity of the ComCat magnitude distribution (Fig. 1) obscures the more complex magnitude distribution revealed when this bias is corrected. This has important implications for calculating parameters like the *b*-value, which assumes an underlying exponential distribution and depends on the mean magnitude above the completeness level of the catalog, so is more sensitive to the frequently occurring small events than the infrequent large ones. Assuming a conservative completeness magnitude of 3.5, the maximum-likelihood estimate of the *b*-value (Bender, 1983) is 0.90 (±0.02) when using the heterogeneous set of ComCat preferred magnitudes, compared to 1.07 (±0.02) when using the uniform

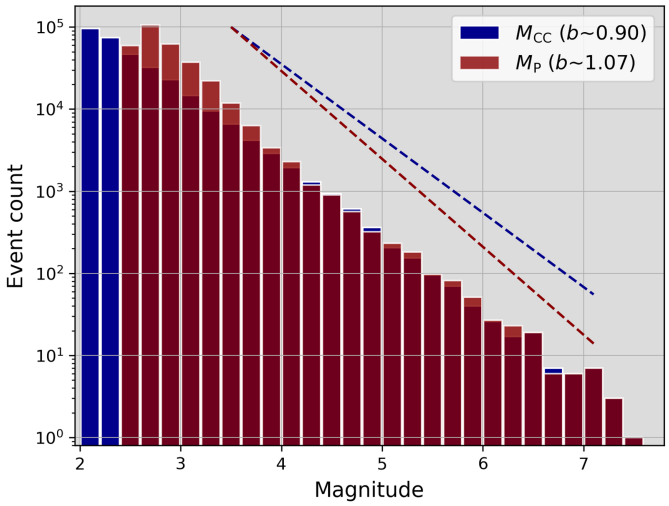

Figure 4. Comparison of frequency–magnitude distributions from the ComCat preferred magnitudes (M_{CC}) and M_P derived from seismic potency. For small earthquakes, the ComCat preferred magnitude M_{CC} underestimates M_P, resulting in a lower apparent b-value for M_{CC} than for M_P (dashed lines). The distribution of M_P is truncated around ~2.7 because the ComCat catalog we analyze only includes events with M_{CC} 2.0 or greater. M_{CC} values in the 2–3 range are systematically corrected to higher values when converting to M_P.

magnitude M_P. Although the numerical difference between these b-value estimates is relatively small, the consequences are important for any statistical parameterization of earthquake processes, including those used in hazard calculations.

Although potency is a desirable metric for parameterizing earthquake size, it is important to acknowledge several current limitations of our study. First, our potency scaling relations were derived from moment estimates in which the assumed rigidity was not documented. To our knowledge, all moment tensor inversion codes used operationally within the western United States assume an effective rigidity in the 30–40 GPa range. The difference between these two extremes translates into an epistemic uncertainty of ±0.06 log units of potency (±0.04 M_P), which could be remedied with clearer documentation in moment tensor solutions. Second, there is a scarcity of small-magnitude data in ComCat with which to develop potency scaling relations. Dedicated studies focused on obtaining potency estimates for small earthquakes (e.g., Ross *et al.*, 2016) could improve the resolution beyond our present means. Third, we neglect regional variations within a given magnitude type (e.g., estimates of M_L published by different monitoring agencies) because these differences are typically smaller and less systematic than the differences between magnitude types, but further studies could investigate this issue in greater detail. Finally, it is important to recognize that potency, even if accurately estimated, only captures the product of fault area and average slip. Earthquakes of equivalent size can produce different ground motions due to different stress drops, rupture velocities, directivity, or other dynamic effects that are not represented by seismic potency (or moment) measurements. We may never be able to characterize all properties of individual earthquakes with perfect accuracy. But we can better represent and quantify the important processes, statistics, and hazards related to earthquakes by better understanding scaling relations between physics-based and instrumental magnitude measurements.

Data and Resources

Earthquake catalog data for this study were obtained from the U.S. Geological Survey (USGS) Comprehensive Catalog (ComCat; https://earthquake.usgs.gov/earthquakes/search/) using the Python library *libcomcat* (https://code.usgs.gov/ghsc/esi/libcomcat-python). Stochastic method simulations were conducted using Python scripts written by the authors and benchmarked against ground motion simulation system (GMSS, https://github.com/Y-Tang99/GMSS1.0). The catalog produced in this study is archived on Zenodo (doi: 10.5281/zenodo.12554989). All websites were last accessed in July 2024. The supplemental material includes a detailed description of the stochastic method implementation used to generate synthetic waveforms, and four additional figures that support the results presented in the main text.

Declaration of Competing Interests

The authors acknowledge that there are no conflicts of interest recorded.

Acknowledgments

The article benefitted significantly from thoughtful and constructive reviews by G. Atkinson and R. Graves, as well as comments from Associate Editor S. Gibbons and Editor-in-Chief K. Koper. The authors thank C. Kreemer for discussions on seismic and geodetic potency scaling relations, and A. Patton and B. Savran for suggestions on the figures. The study was supported by the National Aeronautics and Space Administration (NASA) Award Number 80NSSC24K0736 and the Statewide California Earthquake Center (SCEC) Award Number 24169. SCEC is funded by NSF Cooperative Agreement EAR-2225216 and USGS Cooperative Agreement G24AC00072-00).

References

Aki, K. (1969). Analysis of the seismic coda of local earthquakes as scattered waves, *J. Geophys. Res.* **74,** no. 2, 615–631, doi: 10.1029/JB074i002p00615.

Aki, K. (1972). Earthquake mechanism, *Tectonophysics* **13,** no. 1, 423–446, doi: 10.1016/0040-1951(72)90032-7.

Bakun, W. H. (1984). Seismic moments, local magnitudes, and coda-duration magnitudes for earthquakes in central California, *Bull. Seismol. Soc. Am.* **74,** no. 2, 439–458, doi: 10.1785/BSSA0740020439.

Bakun, W. H., and A. G. Lindh (1977). Local magnitudes, seismic moments, and coda durations for earthquakes near Oroville, California, *Bull. Seismol. Soc. Am.* **67,** no. 3, 615–629, doi: 10.1785/BSSA0670030615.

Bender, B. (1983). Maximum likelihood estimation of b values for magnitude grouped data, *Bull. Seismol. Soc. Am.* **73,** no. 3, 831–851, doi: 10.1785/BSSA0730030831.

Ben-Zion, Y. (1989). The response of two joined quarter spaces to SH line sources located at the material discontinuity interface, *Geophys. J. Int.* **98,** no. 2, 213–222, doi: 10.1111/j.1365-246X.1989.tb03346.x.

Ben-Zion, Y. (2001). On quantification of the earthquake source, *Seismol. Res. Lett.* **72,** no. 2, 151–152, doi: 10.1785/gssrl.72.2.151.

Ben-Zion, Y. (2003). Appendix 2 - Key formulas in earthquake seismology, in *International Handbook of Earthquake and Engineering Seismology, Part B*, W. H. K. Lee, H. Kanamori, P. C. Jennings, and C. Kisslinger (Editors), International Geophysics, Academic Press, Oxford, UK, 1857–1875, doi: 10.1016/S0074-6142(03)80304-2.

Ben-Zion, Y., and L. Zhu (2002). Potency-magnitude scaling relations for southern California earthquakes with 1.0<ML<7.0, *Geophys. J. Int.* **148,** no. 3, F1–F5, doi: 10.1046/j.1365-246X.2002.01637.x.

Boggs, P., and J. Rogers (1990). Orthogonal distance regression, in *Statistical Analysis of Measurement Error Models and Applications*, P. J. Brown and W. A. Fuller (Editors), Proceedings of the AMS-IMS-SIAM Joint Summer Research Conference, June 10–16, 1989, Contemporary Mathematics Vol. 112, 186 pp.

Boore, D. (2003). Simulation of ground motion using the stochastic method, *Pure Appl. Geophys.* **160,** 635–676, doi: 10.1007/PL0001255.

Boore, D. M. (1983). Stochastic simulation of high-frequency ground motions based on seismological models of the radiated spectra, *Bull. Seismol. Soc. Am.* **73,** no. 6A, 1865–1894.

Bormann, P., and J. W. Dewey (2014). The new IASPEI standards for determining magnitudes from digital data and their relation to classical magnitudes, *New Manual of Seismological Observatory Practice 2 (NMSOP-2)*, doi: 10.2312/GFZ.NMSOP-2_IS_3.3.

Efron, B., and R. J. Tibshirani (1994). *An Introduction to the Bootstrap*, CRC Press, Boca Raton, Florida.

Gutenberg, B. (1945a). Amplitudes of P, PP, and S and magnitude of shallow earthquakes*, *Bull. Seismol. Soc. Am.* **35,** no. 2, 57–69, doi: 10.1785/BSSA0350020057.

Gutenberg, B. (1945b). Amplitudes of surface waves and magnitudes of shallow earthquakes*, *Bull. Seismol. Soc. Am.* **35,** no. 1, 3–12, doi: 10.1785/BSSA0350010003.

Hanks, T. C., and D. M. Boore (1984). Moment-magnitude relations in theory and practice, *J. Geophys. Res.* **89,** no. B7, 6229–6235, doi: 10.1029/JB089iB07p06229.

Hanks, T. C., and H. Kanamori (1979). A moment magnitude scale, *J. Geophys. Res.* **84,** no. B5, 2348–2350, doi: 10.1029/JB084iB05p02348.

Herrmann, R. B. (1975). The use of duration as a measure of seismic moment and magnitude, *Bull. Seismol. Soc. Am.* **65,** no. 4, 899–913, doi: 10.1785/BSSA0650040899.

Herrmann, M., and W. Marzocchi (2020). Inconsistencies and lurking pitfalls in the magnitude–frequency distribution of high-resolution earthquake catalogs, *Seismol. Res. Lett.* **92,** no. 2A, 909–922, doi: 10.1785/0220200337.

Hutton, L. K., and D. M. Boore (1987). The ML scale in Southern California, *Bull. Seismol. Soc. Am.* **77,** no. 6, 2074–2094, doi: 10.1785/BSSA0770062074.

Ichinose, G. A., J. G. Anderson, K. D. Smith, and Y. Zeng (2003). Source parameters of Eastern California and Western Nevada earthquakes from regional moment tensor inversion, *Bull. Seismol. Soc. Am.* **93,** no. 1, 61–84, doi: 10.1785/0120020063.

Kanamori, H. (1977). The energy release in great earthquakes, *J. Geophys. Res.* **82,** no. 20, 2981–2987, doi: 10.1029/JB082i020p02981.

Mueller, C. S. (2018). Earthquake catalogs for the USGS National Seismic Hazard Maps, *Seismol. Res. Lett.* **90,** no. 1, 251–261, doi: 10.1785/0220170108.

Richter, C. F. (1935). An instrumental earthquake magnitude scale, 1, *Bull. Seismol. Soc. Am.* **25,** no. 1, 1–32.

Ross, Z. E., Y. Ben-Zion, M. C. White, and F. L. Vernon (2016). Analysis of earthquake body wave spectra for potency and magnitude values: implications for magnitude scaling relations, *Geophys. J. Int.* **207,** no. 2, 1158–1164, doi: 10.1093/gji/ggw327.

Shelly, D. R., K. Mayeda, J. Barno, K. M. Whidden, M. P. Moschetti, A. L. Llenos, J. L. Rubinstein, W. L. Yeck, P. S. Earle, R. Gök, *et al.* (2021). A big problem for small earthquakes: Benchmarking routine magnitudes and conversion relationships with coda envelope-derived Mw in Southern Kansas and Northern Oklahoma, *Bull. Seismol. Soc. Am.* **112,** no. 1, 210–225, doi: 10.1785/0120210115.

Thatcher, W., and T. C. Hanks (1973). Source parameters of southern California earthquakes, *J. Geophys. Res.* **78,** no. 35, 8547–8576, doi: 10.1029/JB078i035p08547.

Utsu, T. (2002). 44 - Relationships between magnitude scales, in *International Geophysics*, W. H. K. Lee, H. Kanamori, P. C. Jennings, and C. Kisslinger (Editors), Vol. 81, Academic Press, Oxford, UK, 733–746, doi: 10.1016/S0074-6142.

Yenier, E., and G. M. Atkinson (2015). An equivalent point-source model for stochastic simulation of earthquake ground motions in California, *Bull. Seismol. Soc. Am.* **105,** no. 3, 1435–1455, doi: 10.1785/0120140254.

Zaliapin, I., and Y. Ben-Zion (2013). Earthquake clusters in southern California I: Identification and stability, *J. Geophys. Res.* **118,** no. 6, 2847–2864, doi: 10.1002/jgrb.50179.

Manuscript received 28 June 2024
Published online 24 September 2024